Bio-Design and Manufacturing (2023) 6:439–450
https://doi.org/10.1007/s42242-023-00238-2

RESEARCH ARTICLE

3D-printed engineered bacteria-laden gelatin/sodium alginate composite hydrogels for biological detection of ionizing radiation

Ziyuan Chen[1] · Jintao Shen[1] · Meng Wei[1] · Wenrui Yan[1] · Qiucheng Yan[1] · Zhangyu Li[1] · Yaqiong Chen[1] · Feng Zhang[1] · Lina Du[1] · Bochuan Yuan[1] · Yiguang Jin[1]

Received: 25 October 2022 / Accepted: 2 February 2023 / Published online: 5 May 2023

Abstract

Nuclear safety is a global growing concern, where ionizing radiation (IR) is a major injury factor resulting in serious damage to organisms. The detection of IR is usually conducted with physical dosimeters; however, biological IR detection methods are deficient. Here, a living composite hydrogel consisting of engineered bacteria and gelatin/sodium alginate was 3D-printed for the biological detection of IR. Three strains of PrecA::*egfp* gene circuit-containing engineered *Escherichia coli* were constructed with IR-dependent fluorescence, and the DH5α strain was finally selected due to its highest radiation response and fluorescence. Engineered bacteria were loaded in a series of gelatin/sodium alginate matrix hydrogels with different rheology, 3D printability and bacterial applicability. A high-gelatin-content hydrogel containing 10% gelatin/1.25% sodium alginate was optimal. The optimal living composite hydrogel was 3D-printed with the special bioink, which reported significant green fluorescence under γ-ray radiation. The living composite hydrogel provides a biological strategy for the detection of environmental ionizing radiation.

Graphic abstract

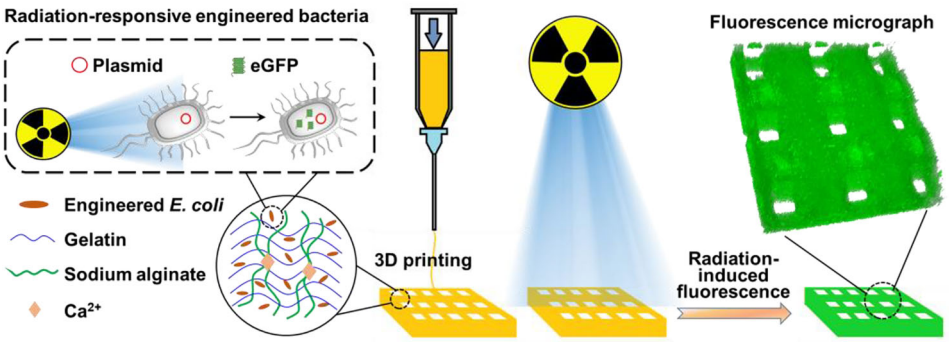

Keywords 3D printing · Alginate · Engineered bacteria · Gelatin · Hydrogel · Ionizing radiation

Introduction

Ionizing radiation (IR) is a phenomenon present in our daily lives, originating from natural and manmade sources. It is a feature of the earth environment and can be an important tool for medical treatment, but uncontrollable environmental radiation may raise concerns about human health and environmental organisms [1–3]. The International Commission on Radiological Protection (ICRP) published a report entitled

✉ Bochuan Yuan
bochuanyuan@sina.com

✉ Yiguang Jin
jinyg@sina.com

[1] Department of Pharmaceutical Sciences, Beijing Institute of Radiation Medicine, Beijing 100850, China

"A framework for assessing the impact of ionizing radiation on non-human species" in 2003 [4]. There are growing concerns about the impact of IR on the environment and natural organisms [5–7]. There were a number of cases wherein wildlife and ecosystems could be exposed to high levels of radiation even when all human beings leave. In fact, in the Fukushima and Chernobyl accidents, aquatic organisms and/or mammals underwent heavy IR, leading to remarkable gene mutations [1]. Thus, the impact of IR on non-human species has become a considerable and important part of international radiological protection recommendations and standards [8, 9]. In addition, the safety of natural and biological environments seriously affects the development of human beings. However, only IR physical dosimeters are available, which are applied to merely detect real-time radiation doses, but do not reflect the irradiation extent of organisms in a period of time. It is urgently needed to find an organism self-dosimeter, i.e., a biological IR detection method, to reflect the irradiation dose anyway.

Bacteria are widespread and simple organisms on Earth. Natural bacteria include pathogens, environmental bacteria and probiotics. They possess the complete cell structure to express functional proteins. Moreover, biotechnology can be applied to modify bacterial genes to express specific proteins, such as green fluorescence protein (GFP) [10]. Engineered bacteria can be employed as detectors to recognize analytes, such as toxic aromatic compounds [11, 12], heavy metals [13–15] and pathogens [16, 17]. Two types of engineered bacteria, *Deinococcus radiodurans* and *Escherichia coli,* have been applied to IR detection, expressing signal proteins induced by IR [18, 19]. However, these engineered bacteria only grow in broth, so they are difficult to adapt to the external environment. Therefore, engineered bacteria need a suitable matrix to provide protection and support for the detection of environmental IR.

Hydrogels are a type of water-swollen three-dimensional (3D) network. Their structural maintenance depends on chemical factors (e.g., covalent bonding and ionic bonding) [20, 21] or physical factors (e.g., electrostatic interactions and hydrogen bonding) [22, 23]. The properties of hydrogels consisting of single materials are usually unsatisfactory, such as low adherence and low mechanical strength. However, we can design functional hydrogels with composites [24, 25]. Gelatin is a common animal-resourced non-toxic biological macromolecule that is usually used to prepare hydrogels for cell culture, wound healing, drug formulation, etc. [26–28]. As a hydrolysate of collagen, gelatin is rich in arginine (R)-glycine (G)-aspartic acid (D) motifs that promote cell attachment, and contains many matrix metalloproteinase recognition sites that are suitable for cell remodeling [29]. Gelatin is one of the most widely used biomaterials for microorganism culture. However, due to the temperature responsiveness of gelatin, it cannot remain solid at the optimal growth temperature for most bacteria. An appropriate cross-linking agent needs to be added. Sodium alginate, as a common natural plant-sourced polymer with good hydrophilicity and biocompatibility, is usually used to formulate small molecular drugs or cells [24, 30]. Sodium alginate can be quickly cross-linked in the presence of Ca^{2+}, Sr^{2+} and other cations. The cross-linking process of sodium alginate is mild, which avoids the inactivation of proteins, enzymes, cells and other active substances. Sodium alginate has good mechanical and biological performance [31]. The two materials are commonly combined to achieve specific functions, such as tissue engineering [32]. One of the outstanding advantages of hydrogels is that they provide a good niche for biomacromolecules and microbes [33]. However, traditional hydrogels are not satisfactory as the matrix of engineered bacteria that usually need a certain of shaped supports, while composite hydrogels may be appropriate as the matrix, but some specific properties such as a desired shape are necessary [34].

3D printing, also called additive manufacturing, is used for manufacturing 3D objects by layer-by-layer addition [35]. 3D printing is a booming technology and is widely used in drug delivery [36], tissue engineering [37] and other fields. 3D printing can customize shapes for different application scenarios, such as gaps, corners and holes, which makes it possible to meet different requirements of detection and application. Organisms are sometimes doped in the matrix as components during 3D printing, called 3D bioprinting, to form functional tissues and organs with proper shapes [38]. In 3D bioprinting, hydrogels are the most common materials, wherein cells or bacteria may grow well due to the network and wet microenvironment of hydrogels [39, 40]. However, few studies have used 3D-printed hydrogels as the matrix of engineered bacteria [41, 42], and no report is related to IR detection. 3D-printed hydrogels provide an opportunity for manufacturing living IR detectors.

Here, we designed a living composite hydrogel, which served as a robust detector for the detection of 10 Gy-grade IR. A PrecA::*egfp* (*recA* promoter driving eGFP expression) gene circuit as the IR detection component was constructed and transferred to three strains of *E. coli*. An optimal engineered *E. coli* strain was screened out according to the detection performance. Meanwhile, a series of gelatin–sodium alginate matrix hydrogels were prepared, and their mechanical properties, rheology, 3D printability and applicability were explored with loading of the bacteria. An optimal gelatin–sodium alginate matrix hydrogel was mixed with the engineered *E. coli* to form bioink, which was 3D-printed to grids. The γ-ray responsive performance of this living 3D-printed hydrogel was explored, and the relationship between the irradiation dose and fluorescent intensity was profiled.

Materials and methods

Materials

TransStart® FastPfu Fly DNA Polymerase, T4 DNA Ligase and nuclease-free water were purchased from TransGen Biotech Co., Ltd. (Beijing, China). Endonucleases KpnI and ClaI were obtained from New England Biolabs, Inc. (MA, USA). Agar was provided by AOBOX Biotechnology Co., Ltd. (Beijing, China). dNTPs (10 mM), Luria–Bertani (LB) broth, chloramphenicol and ampicillin were purchased from Beijing Solarbio Science & Technology Co., Ltd. (Beijing, China). Gelatin from porcine skin (type A, gel strength: ~ 300 g Bloom) was purchased from Sigma-Aldrich (USA), and sodium alginate (1% solution, viscosity: 200–500 mPa·s) was purchased from Adamas-beta (Shanghai, China). Cellulose nanocrystal powders were provided by ScienceK (Zhejiang, China). Calcium chloride anhydrous ($CaCl_2$) was obtained from Xilong Scientific Co., Ltd. (Guangdong, China). Trisodium citrate dihydrate was purchased from Sinopharm Chemical Reagent Co., Ltd. (Beijing, China). The E.Z.N.A.® Plasmid Mini Kit I was purchased from Omega (USA). The DNA Clean & Concentrator™-5 Kit and Zymoclean™ Gel DNA Recovery Kit were purchased from ZYMO RESEARCH (USA). All other chemicals were of analytical grade and were used without further purification. Deionized water was prepared using a Heal Force Super NW Water System (Shanghai Canrex Analytic Instrument Co., Ltd., Shanghai, China) and was used consistently.

Plasmids, bacterial strains, media and growth conditions

The primers, plasmids and *E. coli* strains used in this study are described in Table 1. *E. coli* was grown at 37 °C in LB broth or on LB plates solidified with 2% agar. If necessary, appropriate antibiotics (100 μg/mL ampicillin or 50 μg/mL chloramphenicol) were added to the solid or liquid media for the screening of engineered *E. coli*. Gene transformations of plasmids into *E. coli* were conducted using the $CaCl_2$ method described in the literature [19]. All bacterial irradiation experiments were performed at room temperature.

Construction of plasmids and engineered strains

A radiation-responsive plasmid, pEC-PrecA::*egfp*, was constructed as follows. An original vector, pSB3C5-MCS-*egfp*, was digested to its linear state using an enzyme mixture of KpnI and ClaI. The promoter region of the *recA* gene fragment in the *E. coli* wild-type (ATCC25922) genome was obtained by polymerase chain reaction (PCR) with the primers in Table 1, which had the restriction enzyme sites, i.e., the KpnI and ClaI sites. The above deoxyribonucleic acid (DNA) fragments were digested using an enzyme mixture of KpnI and ClaI, and the products were ligated into the same sites as the linearized vector fragments to obtain pEC-PrecA::*egfp*.

pEC-PrecA::*egfp* was transformed into three strains of *E. coli*, i.e., DH5α, BL21(DE3) and ATCC25922 (wild type, WT), and their transformants obtained by chloramphenicol resistance selection were designated EC-1, EC-2 and EC-3, respectively. The plasmid pJ61002::*egfp,* which constitutively expressed eGFP, was transformed into *E. coli* DH5α, and the transformant obtained by ampicillin resistance selection was designated EC-4. EC-4 was used as the positive control in the subsequent experiments.

Radiation tolerance test of engineered *E. coli*

Three strains of engineered *E. coli*, including EC-1, EC-2 and EC-3, were cultured in LB broth supplemented with 50 μg/mL chloramphenicol in an oscillating incubator until the OD_{600} reached 0.5–0.6 (the exponential phase). The OD_{600} of bacterial suspensions was measured using a multifunctional microplate reader (Spark, Tecan, Swiss). EC-1, EC-2 and EC-3 were randomly divided into six groups (each group containing 5 mL of bacterial suspension). All of them were irradiated with 0 (non-irradiated), 10, 30, 50, 80 and 100 Gy using a ^{60}Co γ-ray source (Beijing Institute of Radiation Medicine, Beijing, China) at a dose rate of 236.56 cGy/min. An aliquot (50 μL) of irradiated bacterial suspensions was spread on a solid LB plate (n=3) supplemented with 50 μg/mL chloramphenicol followed by incubation at 37 °C. The survival rates of bacteria were calculated according to colony counting.

eGFP expression measurement in engineered *E. coli* following irradiation

Engineered *E. coli* was cultured by oscillating at 37 °C to the exponential phase in LB broth supplemented with 50 μg/mL chloramphenicol. The above *E. coli* was exposed to 10 Gy γ-rays and then cultured by oscillation for 1 h. The continued culture of irradiated *E. coli* is called recovery. After 1 h of recovery, a drop of bacterial suspension was spread on a glass slide and observed with a fluorescence microscope (ECLIPSE Ti-U, Nikon, Japan). The engineered *E. coli* irradiated with 25 Gy γ-ray was conducted with eGFP western blotting according to the standard protocol [43], and the untreated EC-4 was used as the positive control.

EC-1, EC-2 and EC-3 grown to the exponential phase were randomly divided into seven groups and irradiated with 0 (non-irradiated), 10, 20, 30, 40, 50 and 60 Gy. The bacteria were incubated at 37 °C, and relative fluorescence units (RFUs) and OD_{600} were detected (n=56) at the predetermined time points (1, 2, 3, 4, 5, 6, 7 and 8 h). RFU was

Table 1 Primers, plasmids and strains used in this study

Type	Name	Description	Source
Primers	dEC-PrecA-F	5′-CCATCGATAGCCAAAGCGCAGATGAT-3′	This study
	dEC-PrecA-R	5′-GGGGTACCTTTTACTCCTGTCATGCCG-3′	
Plasmids	pSB3C5-MCS-*egfp*	Template plasmid bearing *egfp* gene, p15A ori and Cm^R	SyngenTech
	pEC-PrecA::*egfp*	Derivative of pSB3C5-MCS-EGFP bearing inducible promoter PrecA and *egfp* gene, p15A ori and Cm^R	This study
	pJ61002::*egfp*	Template plasmid bearing constitutive promoter (J61002), *egfp* gene, pUC ori and Amp^R	SyngenTech
Strains	*E. coli* DH5α	F-, *Φ80lacZ·ΔM15·f(lacZYA-argF)U169 deoR recA1 endA1 hsdR17(rk,-mk+) phoA supE44 thi-1 gyrA96 relA1*	Biomed
	E. coli BL21(DE3)	F-, *ompT hsdSB(rB-mB-)galdcm(DE3)*	Biomed
	E. coli wild type	ATCC25922 (O:6, Biotype 1)	ATCC
	EC-1	*E. coli* DH5α bearing pEC-PrecA::*egfp*	This study
	EC-2	*E. coli* BL21(DE3) bearing pEC-PrecA::*egfp*	This study
	EC-3	*E. coli* wild type (ATCC25922) bearing pEC-PrecA::*egfp*	This study
	EC-4	*E. coli* DH5α bearing pJ61002::*egfp*	This study

detected using a multifunctional microplate reader at an excitation wavelength of 485 nm and an emission wavelength of 535 nm. The relative fluorescence intensity (RFI, meaning RFU/OD_{600}) was calculated. The relationships between the RFI and irradiation dose and between the RFI and recovery time were constructed.

Preparation of hydrogels

Three materials—gelatin, sodium alginate and cellulose nanocrystals (CNCs)—were dissolved or dispersed and then mixed in proportion. Gelatin was dissolved in water by agitation at 50 °C to obtain a gelatin solution. Sodium alginate was dissolved in water with stirring at room temperature, while CNCs were dispersed in water by sonication using an ultrasonic cleaner (KW-822D, Kejeme Experimental Instruments Co., Ltd., China). The four formulations of hydrogel were (a) low-gelatin-content alginate hydrogels (LGA, 5% gelation and 1.25% sodium alginate) from 0.6 g of gelatin in 4 mL and 0.15 g of sodium alginate in 8 mL, (b) high-gelatin-content alginate hydrogels (HGA, 10% gelation and 1.25% sodium alginate) from 1.2 g of gelatin in 4 mL and 0.15 g of sodium alginate in 8 mL, (c) low-gelatin-content alginate CNC hydrogels (LGAC, 5% gelation, 1.25% sodium alginate and 0.25% CNCs) from 0.6 g of gelatin in 4 mL, 0.15 g of sodium alginate in 7 mL and 0.03 g of CNCs in 1 mL, and (d) high-gelatin-content alginate CNC hydrogels (HGAC, 10% gelation, 1.25% sodium alginate and 0.25% CNCs) from 1.2 g of gelatin in 4 mL, 0.15 g of sodium alginate in 7 mL and 0.03 g of CNCs in 1 mL. The four hydrogels were cured after immersion in 1% (0.01 g/mL) $CaCl_2$ solutions for 2 min.

Sol–gel transition test

The formation of hydrogels was tested with the tube-inverting method [44]. The hydrogel precursors were added into glass vials (10 mL). The vials were allowed to equilibrate at 4, 26 and 37 °C for 10 min, respectively. The vials were tilted to observe the physical states of the hydrogels. Then, 2 mL of 1% $CaCl_2$ solutions was separately added into these vials under hand shaking and maintained for 2 min. The sol–gel transition was observed.

Scanning electron microscopy

The hydrogels were cryo-fractured in liquid nitrogen and then freeze-dried in a lyophilizer (LGJ-30F, Songyuan Huaxing Technology Develop Co., Ltd., China). The lyophilized samples were coated with a thin gold layer on the cross sections using an ion sputtering instrument (SBC-12, KYKY Technology Co., Ltd., China) and observed under a scanning electron microscope (SEM, EmCtafts CUBE II, 20 kV, Korea).

Rheological test of hydrogels

The hydrogels were prepared into cylinders (25 mm in diameter×2 mm in height) for rheological tests. The rheological properties of the hydrogels were measured with a rheometer (HAAKE MARS40, Thermo Fisher Scientific, USA). The storage modulus (G') and loss modulus (G'') were

recorded. Time sweep tests within 1 h were performed at a constant strain of 0.5% and a frequency of 10 Hz. Temperature sweep tests were performed at a constant strain of 0.5% and a frequency of 10 Hz at various temperatures (4–40 °C), rising at a constant rate of 1 °C/min.

Mechanical property test of hydrogels

Hydrogels were prepared in cubes (15 mm in length × 15 mm in width × 3 mm in height) for the compression test. The mechanical properties of the hydrogels were measured with a universal experimental instrument (INSTRON 5982, Instron, USA) by crushing them with a crosshead speed of 0.5 mm/min.

3D printing and printability test of hydrogels

Hydrogels were printed using an extruded 3D printer (Regenova sparrow, Regenovo, Hangzhou, China). Prior to printing, the hydrogel precursors of LGA, LGAC, HGA or HGAC were transferred into a 5-mL silo injector with a 22-G dispensing needle. 3D printing was performed using the extrusion printer. For the printing of the LGA, the temperature of the silo injector and needle was set to 23 °C, a constant printing speed of 11 mm/s was kept, and a constant pressure of 0.15 MPa was maintained. The printing parameters of LGAC were the same as those of LGA except for adjusting the pressure to 0.1 MPa. For the printing of HGA, the above parameters were 27 °C, 13 mm/s and 0.15 MPa, respectively. The printing parameters of HGAC were the same as those of HGA except for the feed rate of 12 mm/s. The patterns (15 mm × 15 mm) were designed and sliced using BioPrinterApp software. The hydrogels were printed on a 4 °C platform with 1, 2, 5 and 10 layers (0.3 mm high per layer), respectively, followed by immersion in 1% $CaCl_2$ solutions for 2 min to cure. The solidified hydrogels were observed under a microscope (Y-TV55, Nikon, Japan). Different shapes of the printed hydrogels were tried, including the square grid (15 mm × 15 mm × 10 layers), the radiation-like structure (60 mm × 60 mm × 10 layers) and the tai chi structure (50 mm × 50 mm × 10 layers). Methylene blue was doped for clear observation.

Survival rate and fluorescence detection of *E. coli* in hydrogels

Gelatin powders and alginate powders were spread on a plate followed by ultraviolet (UV) sterilization. Ampicillin was added to the HGA precursor at 100 μg/mL. EC-4 cells were incubated at 37 °C to the exponential phase and collected after centrifugation. The collected bacterial suspension was added following agitation for 10 min at 37 °C to obtain the EC-4 bioink. The bioink was printed with 10 layers as described above. The whole process was performed on a clean bench (VD-850, Zhucheng Yuyang Food Machinery Co., Ltd., China). The printed hydrogels were weighed and incubated at 37 °C for 0, 1, 2 and 3 days (n=3). Equal-weight EC-4 suspensions were used as the control. The hydrogels were dissolved in 5% (0.05 g/mL) sodium citrate solutions, centrifuged (4000 × g, 5 min) and suspended in 1 mL of LB broth. The survival rate and RFI were detected. The relationships between the numbers of EC-4 and RFI or incubation time were constructed. The hydrogels were observed under a laser confocal microscope (Stellaris 5 SR, Lecia, Germany).

Fluorescence assays for living composite hydrogels

Living composite hydrogels were printed with EC-1 bioink and 10 layers as described above. The living composite hydrogels were exposed to γ-ray radiation of 0, 10, 30 and 50 Gy (n=3). The RFI after 4 h of recovery was detected, and the relationship between the RFI and irradiation dose was constructed. The living composite hydrogels exposed to 50 Gy radiation and 4 h of recovery were observed under a laser confocal microscope.

Statistical evaluation

All statistical analyses were performed using SPSS software (version 26.0, International Business Machines Corporation, Armonk, NJ, USA), and P<0.05 indicated significant differences.

Results and discussion

Successful construction of radiation-responsive engineered *E. coli* strains

No signaling pathway has been found in microbial cells to be directly activated by IR, so a feasible alternative is the *recA*-dependent SOS response of DNA repair. It is a well-recognized mechanism widely used in the construction of radiation-responsive engineered bacteria [45, 46]. Briefly, IR causes damage to DNA in microbial cells, resulting in DNA single-strand breaks. Single-stranded DNA (ssDNA) recruits inactive RecA and adenosine triphosphate (ATP) to assemble the RecA-ssDNA filament, and then, RecA is converted into an active and specific protease to cleave the LexA repressor. Cleaved LexA repressors detach from the SOS box in DNA, leading to transcription of the repressed genes (Fig. 1) [47]. Hence, IR is reported by the production of fluorescence when the fusion of SOS regulator and *egfp* occurs. In this study, *E. coli* was selected as a subject for engineering due to its clearest genetic background.

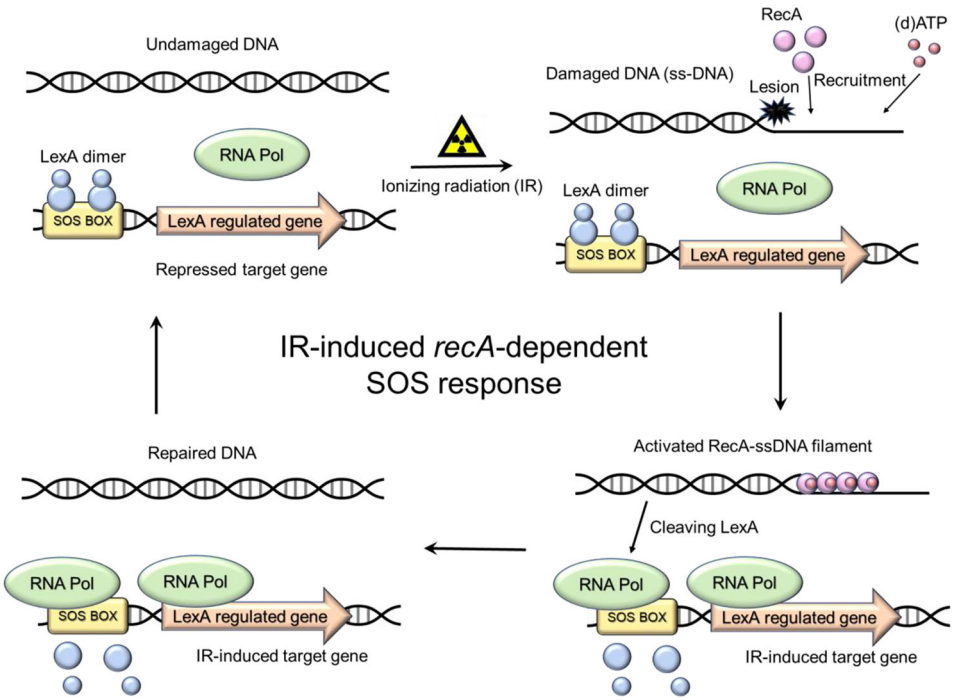

Fig. 1 Mechanism of the ionizing radiation (IR)-induced *recA*-dependent SOS response in *E. coli*. RNA Pol: RNA polymerase; LexA dimer: a protein repressor bound to the SOS box; SOS box: cis-acting element regulating tandem gene expression; RecA: a DNA repair protease

The fused gene circuit of the *recA* promoter driving *egfp* expression was constructed and cloned into the plasmid (Fig. 2a) according to the reported process [48]. Previous studies might overlook the varied effects of the different strains belonging to the same species on the reported performance, and the strains of different genotypes would yield differential responsive capabilities due to multiple genes participating in the induction of SOS response, especially critical mutations located in the pathway proteins. Thus, the plasmid pEC-PrecA::*egfp* was transformed into three strains of *E. coli*, i.e., DH5α, BL21(DE3) and ATCC25922 (wild type, WT), obtaining three genotypes of engineered *E. coli* designated EC-1 (*E. coli*-DH5α-PrecA::*egfp*), EC-2 (*E. coli*-BL21-PrecA::*egfp*) and EC-3 (*E. coli*-WT-PrecA::*egfp*), respectively. The engineered *E. coli* strain showed significant green fluorescence after 10 Gy γ-ray radiation and 1 h recovery, indicating the successful construction of radiation-responsive engineered *E. coli* strains (Fig. 2b). Moreover, western blotting also demonstrated the high expression of eGFP in the strains induced by 25 Gy γ-ray radiation (Fig. S1 in Supplementary Information).

Radiation-reported performance of engineered E. coli

The IR tolerance of engineered *E. coli* must be known at the beginning. All three irradiated strains showed a decreased survival rate featuring logarithmic function trends. Among them, EC-3 possessed the highest sensitivity to γ-rays; i.e., EC-3 was the easiest strain to die (Fig. 2c). Moreover, we found that high-dose (more than 60 Gy) radiation led to serious deaths with a survival rate approaching zero. Therefore, 60 Gy was the top limitation for engineered bacteria and living composite hydrogels.

The rapid recovery of irradiated engineered bacteria is important for future living composite hydrogels. After a very high dose (60 Gy) of radiation, the three engineered bacteria, EC-1, EC-2 and EC-3, showed different recovery profiles reflected in the RFI. As mentioned above, EC-3 had difficulty in recovering and tended to die (Fig. 2d). However, EC-1 and EC-2 basically showed recovery profiles depending on recovery time, although the death profiles appeared in the first hour. Similar results were also shown when radiation lower than 60 Gy was applied (Fig. S2 in Supplementary Information). Moreover, EC-1 exhibited an almost linear relationship between the RFI and recovery time in the range of 2–8 h, but EC-2 did not. The linear relationship of EC-1 would be beneficial to radiation detection using living composite hydrogels. Moreover, compared with the non-irradiated group, the RFI of EC-1 in the irradiated group showed a significant difference (P<0.001) after at least 2 h of recovery, indicating that ionizing radiation significantly induced the generation of fluorescence in EC-1 (Fig. S3 in Supplementary Information). We finally used the 4-h recovery of EC-1 when detecting ionizing radiation.

Properties of matrix hydrogels

Bacteria, including engineered bacteria, must grow in the appropriate environment [49]. Hydrogels may be the most

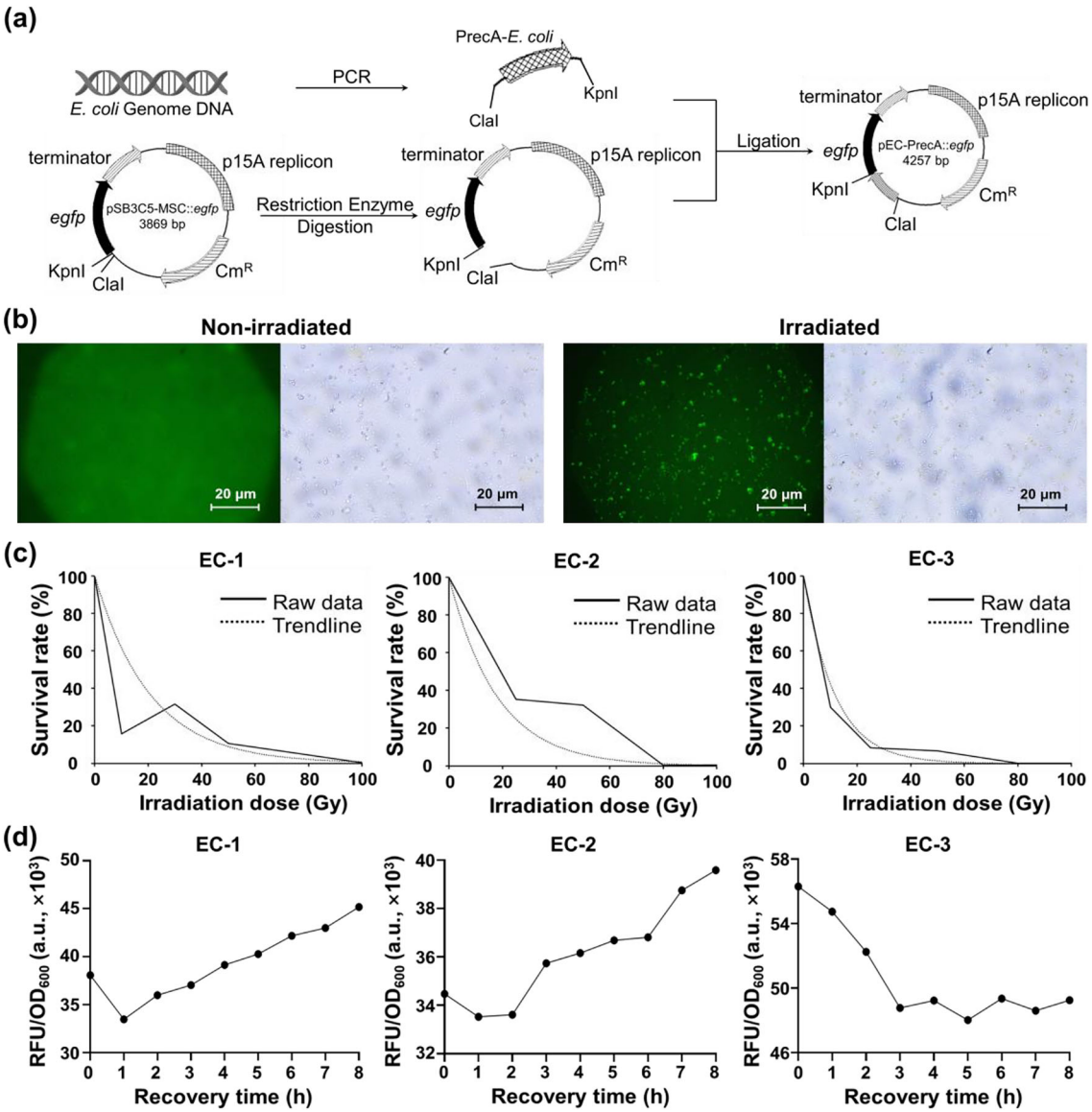

Fig. 2 Construction and properties of the plasmid and engineered bacteria. **a** Construction process of plasmid pEC-PrecA::*egfp*. **b** Fluorescence images and radiation response of recovered engineered *E. coli* depending on radiation. **c** Survival rates of three engineered *E. coli* strains (EC-1, EC-2 and EC-3) with ^{60}Co radiation of 0 to 100 Gy. **d** Relationships of the relative fluorescence intensity (RFI) and the recovery time of engineered *E. coli* after 60 Gy radiation

common matrix for the growth of engineered bacteria because they can provide a variety of conditions, such as biocompatibility, nutrition and robustness. Gelatin-based hydrogels have been widely used in tissue engineering and 3D cell culture, indicating that gelatin has good biocompatibility [50]. In this study, gelatin was used as the basic component of matrix hydrogels. However, gelatin may become fluid when the temperature rises. Therefore, it is necessary to add a cross-linking agent to maintain the structure of hydrogels in a high-temperature environment. Sodium alginate features fast cross-linking and good biocompatibility and is widely used as the cross-linking agent in bioprinting [31]. In addition, CNCs are used as one component for bioprinting because they can provide additional mechanical properties to hydrogels [51]. Therefore, gelatin, sodium alginate and CNCs were selected as the components of the matrix hydrogels.

Four types of matrix hydrogels, including LGA, LGAC, HGA and HGAC, maintained solids at 4 °C independent of 1% $CaCl_2$ because of the solid gelatin (Fig. 3a). However, at 26 °C, LGA and LGAC appeared as liquids, although they transformed to solids upon $CaCl_2$ addition. The low content

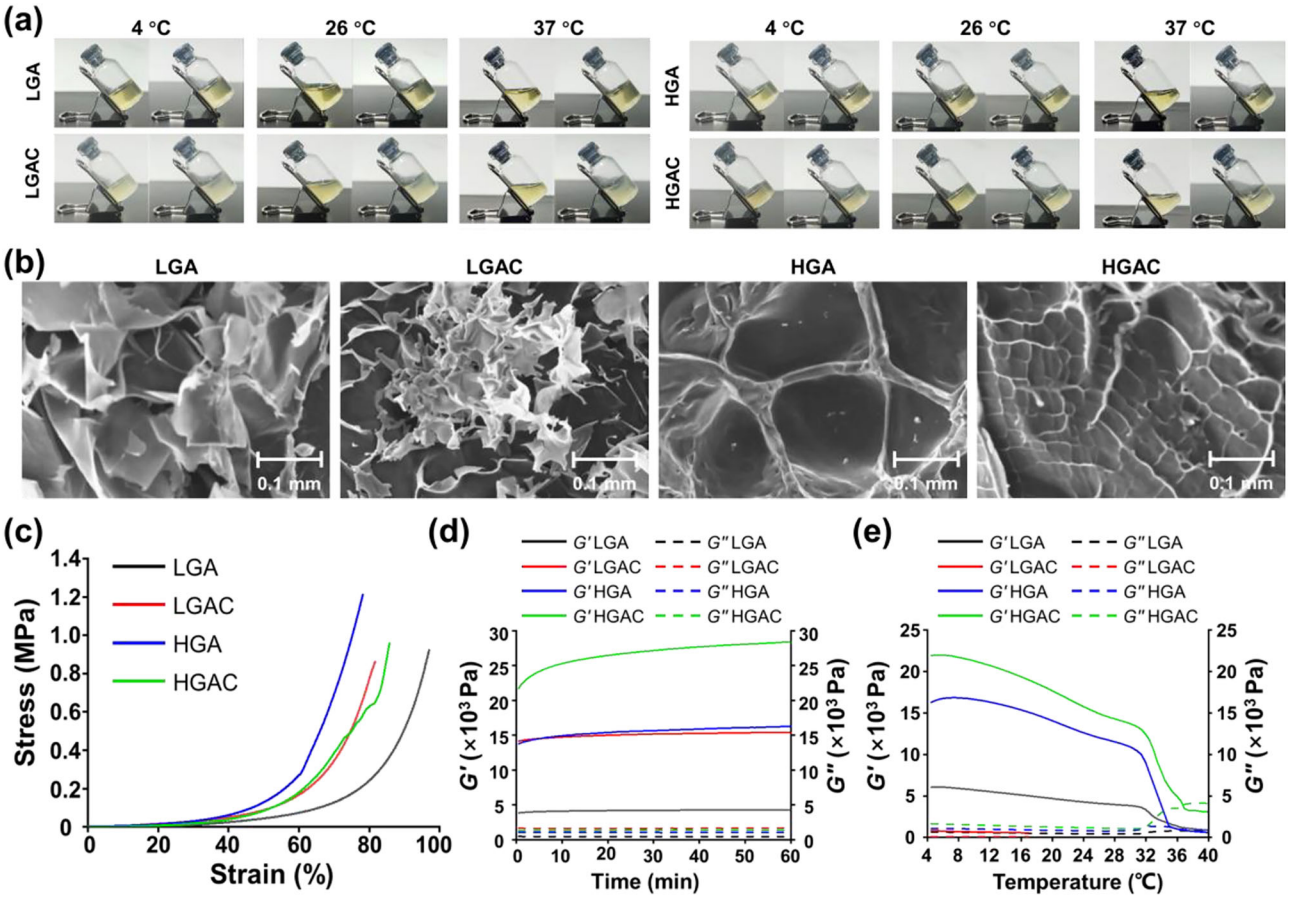

Fig. 3 Characteristics of matrix hydrogels. **a** Fluidity of the hydrogels before (left images) and after (right images) cross-linking using 1% $CaCl_2$ at various temperatures. **b** Scanning electron microscopy (SEM) images of the hydrogels. **c** Compression performance of the hydrogels. **d** Rheological properties of the hydrogels (time sweep experiments with constant frequency and strain). **e** Rheological properties of the hydrogels (temperature sweep experiments from 4 to 40 °C with a constant rate of 1 °C/min)

of gelatin in LGA and LGAC contributed to this result. In contrast, HGA and HGAC maintained solids at 26 °C due to the high content of gelatin. Moreover, all the hydrogels were fluids at 37 °C and kept solids with the addition of $CaCl_2$, which cross-linked the alginate (Fig. 3a). The addition of CNCs did not influence the state of the composite hydrogels.

The lyophilized hydrogels had different microscale morphologies, as shown by SEM (Fig. 3b). LGA and LGAC showed broken microscale structures because the low content of gelatin could not support the hydrogel structure. In contrast, the lyophilized HGA and HGAC had many homogenous pores, although the pores in HGAC were much smaller than those in HGA. The pores or channels in hydrogels are beneficial to the uptake and exchange of embedded bacteria; however, very small pores might limit the transportation of chemicals. Therefore, HGA may be a better selection.

The robustness of composite hydrogels determines their adaptability in the natural environment. Among the matrix hydrogels, HGA had the highest stress of 1.2 MPa and the smallest strain of 78% (Fig. 3c), indicating its good robustness. The higher the storage modulus (G') is, the more rigid the solid hydrogel is. In contrast, the loss modulus (G'') indicates the fluid state of the hydrogels, and the lower the G'' is, the more flowing the hydrogels are. Two modes, including the time sweep experiments and the temperature sweep experiments, showed that HGAC maintained the highest G' although all four hydrogels had a similar G'', and HGA also maintained a high G' compared with the G''. Moreover, the temperature sweep experiments showed that all the hydrogels became unstable at high temperature, which could be attributed to the property of gelatin (Figs. 3d and 3e). Nevertheless, all the hydrogels had reliable stability at room temperature (20 °C). In addition, LGAC completely broke as the temperature increased (Fig. S4 in Supplementary Information). Therefore, due to the good mechanical strength and simple formulation, HGA was the optimal matrix hydrogel as the next experimental subject.

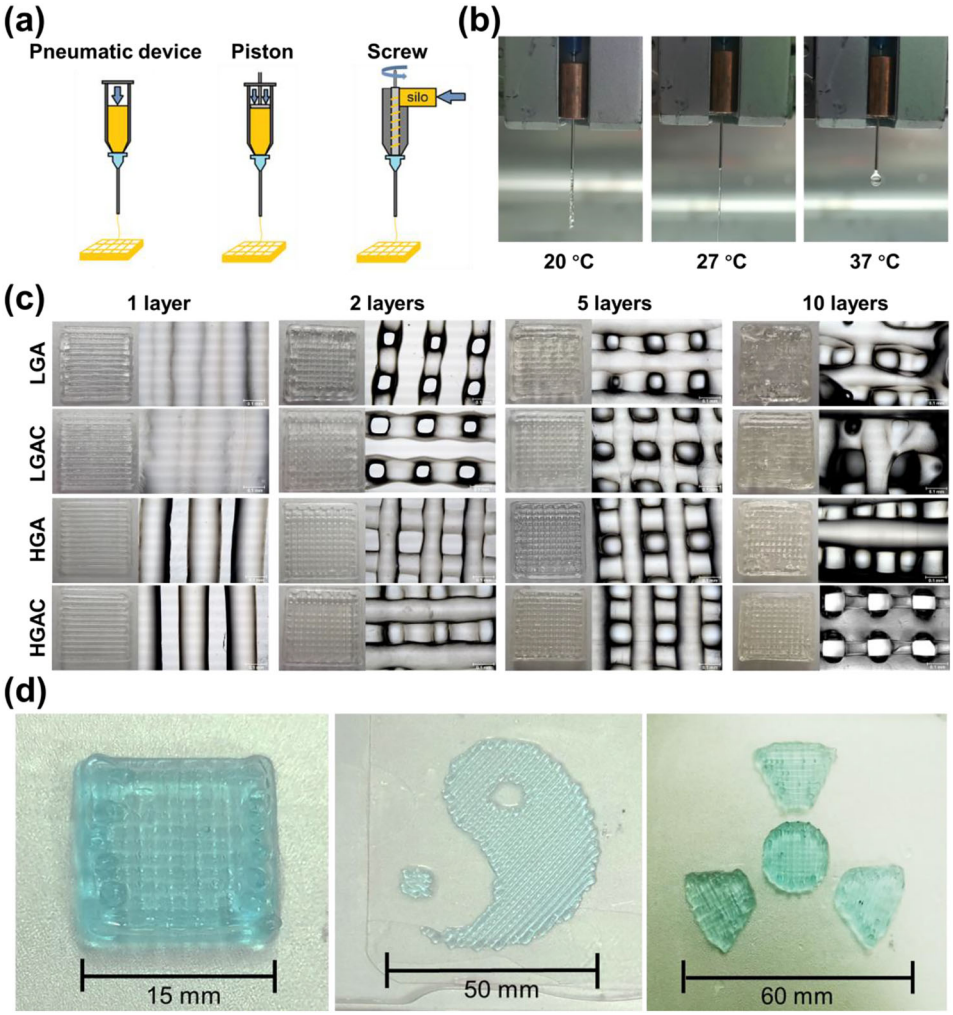

Fig. 4 3D printing of matrix hydrogels. **a** Illustration of the printing process of the extrusion-based printer. **b** Extrusion states of HGA at various temperatures. **c** Appearance and microscopic images of the grids of composite hydrogels with different layers. **d** 3D-printed HGA structures of different shapes, including the square grid, the tai chi structure and the radiation-like structure

Printability of hydrogels

The printability of hydrogels for 3D printing can be evaluated using a pneumatic extrusion-based printer [52]. In this study, the extrusion state of HGA depended on the temperature of the silo (Fig. 4a). At 37, 27 and 20 °C, the extruded HGA appeared as liquid droplets, continual filaments and linked knots (Fig. 4b), respectively, which was related to the sol–gel transition of gelatin at different temperatures. Certainly, the continual filaments were appropriate for 3D printing, and the silo temperature was controlled to nearly 27 °C. The other hydrogel precursors had similar results. To make the engineered bacteria grow well, multiple layers of hydrogels are needed. The four composite hydrogels were printed from 1 to 10 layers. All the hydrogels had well-organized grids within 5 layers (Fig. 4c). However, collapsed grids appeared in the hydrogels with low-content gelatin, i.e., LGA and LGAC, when 10 layers were printed. In contrast, the grids of HGA and HGAC always maintained completeness even to 10 layers where the height was 4 mm (Fig. S5 in Supplementary Information), and these grids allowed many squeezes without fracture (see Supplementary Information). Moreover, more morphologies than grids of HGA were 3D-printed, such as the tai chi structure and the radiation-like structure (Fig. 4d), which indicated the high adaptability of 3D-printed composite hydrogels.

Fluorescence stability and radiation response of living composite hydrogels

The fluorescence stability of living composite hydrogels is important for sensing radiation. EC-4 bearing the pJ61002::*egfp* plasmid was used, which constitutively expressed *egfp*. The fluorescence intensities of EC-4 in both the hydrogel and the LB broth showed initial decreases and then maintained similar stable profiles (Fig. 5a). Therefore, the hydrogel did not influence the survival of engineered bacteria. Moreover, confocal fluorescence images showed the strong and homogenous green fluorescence of the hydrogel (Fig. 5b), indicating that the engineered bacteria were well

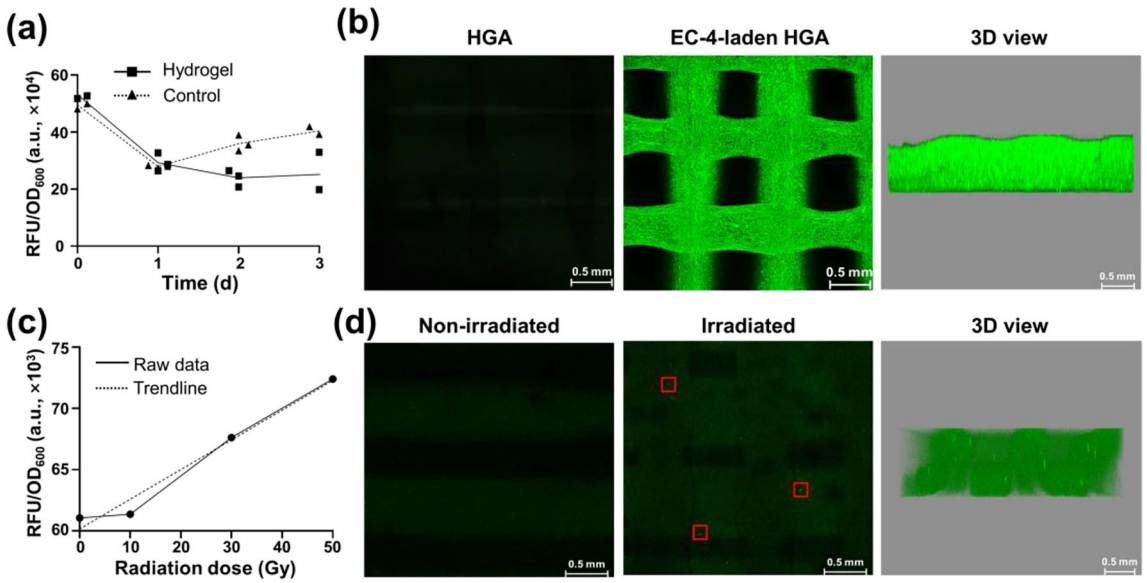

Fig. 5 Fluorescence of living composite hydrogels. **a** Relative fluorescence intensity (RFI) of EC-4 in the hydrogels and Luria–Bertani (LB) broth depending on days. **b** Confocal fluorescence micrographs of EC-4-laden HGA. **c** Radiation sensing of living composite hydrogels. **d** Confocal fluorescence micrographs of the radiation-responsive hydrogel

distributed in the hydrogel. Moreover, the EC-1-laden living composite hydrogel showed remarkable fluorescence under γ-ray radiation compared to the background of the hydrogel (Figs. 5c and 5d), indicating that the radiation-responsive hydrogel was successfully constructed.

The above results proved the feasibility of ionizing radiation detection using the living hydrogel. Living hydrogels can be used in the detection of radiation source leakage, nuclear accidents, accidental exposure, etc. The current living hydrogel was dissolved in sodium citrate to release the engineered bacteria loaded in it, leading to easy fluorescence intensity reading of bacteria by a microplate reader to achieve ionizing radiation detection in real applications. A kit and its standard operating procedure can be further designed to make it easier for operators. Moreover, the engineered bacteria, i.e., the detection component of the living hydrogel, can be further optimized to achieve a lower detection limit by screening gene elements and optimizing gene circuits. It is expected to detect low-dose ionizing radiation more accurately to fit more application scenarios.

Conclusions

Radiation biological detection is a scientific problem due to the deficiency of radiation-responsive engineered bacteria and, more importantly, the support of engineered bacteria. Hydrogels and 3D printing provide opportunities for addressing this problem. Natural biomaterials, i.e., gelatin and alginate, can form an appropriate matrix hydrogel for 3D printing and then provide good support for the survival of radiation-responsive engineered bacteria due to the good biocompatibility and mechanical properties of the matrix. Finally, a living composite hydrogel can be prepared for biological detection of ionizing radiation. This study provides a new paradigm of combinational applications of biomaterials, 3D printing and engineered bacteria, and a new method for evaluating IR-induced biological injury.

Supplementary Information The online version contains supplementary material available at https://doi.org/10.1007/s42242-023-00238-2.

Acknowledgements This work was supported by the Special Program for Capability Promotion.

Author contributions ZYC and YGJ conceived the study; ZYC, FZ and BCY curated the data; ZYC, JTS and QCY performed the formal analysis; BCY and YGJ acquired the funding; ZYC and MW conducted the investigation; ZYC, ZYL and BCY contributed to methodology; LND and YGJ were responsible for resources; LND, BCY and YGJ took part in supervision; WRY, JTS and YQC carried out validation; ZYC wrote the original draft; ZYC, JTS, BCY and YGJ wrote, reviewed and edited the manuscript.

Declarations

Conflict of interest The authors declare that they have no conflict of interest.

Ethical approval This study does not contain any studies with human or animal subjects performed by any of the authors.

References

1. Hirose K (2020) Atmospheric effects of Fukushima nuclear accident: a review from a sight of atmospheric monitoring. J Environ Radioact 218:106240. https://doi.org/10.1016/j.jenvrad.2020.106240
2. Brumfiel G, Fuyuno I (2012) Japan's nuclear crisis: Fukushima's legacy of fear. Nature 483:138–140. https://doi.org/10.1038/483138a
3. Gorobets A (2016) Chernobyl anniversary: Ukraine should cut back nuclear power. Nature 534:37. https://doi.org/10.1038/534037e
4. Valentin J (2003) A framework for assessing the impact of ionising radiation on non-human species. Ann ICRP 33(3):207–266. https://doi.org/10.1016/S0146-6453(03)000
5. Pentreath RJ (1999) A system for radiological protection of the environment: some initial thoughts and ideas. J Radiol Prot 19:117–128. https://doi.org/10.1088/0952-4746/19/2/302
6. International Atomic Energy Agency (2002) Ethical considerations in protecting the environment from the effects of ionizing radiation: a report for discussion. IAEA, Vienna
7. Oughton DH (2016) Ethical foundations of environmental radiological protection. Ann ICRP 45(1 Suppl):345–357. https://doi.org/10.1177/0146645316639836
8. International Commission on Radiological Protection (2007) The 2007 recommendations of the international commission on radiological protection. Ann ICRP, Oxford
9. International Atomic Energy Agency (2014) Radiation protection and safety of radiation sources: international basic safety standards. IAEA, Vienna
10. Martinez AR, Heil JR, Charles TC (2019) An engineered GFP fluorescent bacterial biosensor for detecting and quantifying silver and copper ions. Biometals 32:265–272. https://doi.org/10.1007/s10534-019-00179-3
11. Roy R, Ray S, Chowdhury A et al (2021) Tunable multiplexed whole-cell biosensors as environmental diagnostics for ppb-level detection of aromatic pollutants. ACS Sens 6:1933–1939. https://doi.org/10.1021/acssensors.1c00329
12. Xue H, Shi H, Yu Z et al (2014) Design, construction, and characterization of a set of biosensors for aromatic compounds. ACS Synth Biol 3:1011–1014. https://doi.org/10.1021/sb500023f
13. Bereza-Malcolm LT, Mann G, Franks AE (2015) Environmental sensing of heavy metals through whole cell microbial biosensors: a synthetic biology approach. ACS Synth Biol 4:535–546. https://doi.org/10.1021/sb500286r
14. Jia X, Zhao T, Liu Y et al (2018) Gene circuit engineering to improve the performance of a whole-cell lead biosensor. FEMS Microbiol Lett 365:fny157. https://doi.org/10.1093/femsle/fny157
15. Mendoza JI, Soncini FC, Checa SK (2020) Engineering of a Au-sensor to develop a Hg-specific, sensitive and robust whole-cell biosensor for on-site water monitoring. Chem Commun 56:6590–6593. https://doi.org/10.1039/d0cc01323d
16. Wu Y, Wang C, Wang D et al (2021) A whole-cell biosensor for point-of-care detection of waterborne bacterial pathogens. ACS Synth Biol 10:333–344. https://doi.org/10.1021/acssynbio.0c00491
17. Struss A, Pasini P, Ensor CM et al (2010) Paper strip whole cell biosensors: a portable test for the semiquantitative detection of bacterial quorum signaling molecules. Anal Chem 82:4457–4463. https://doi.org/10.1021/ac100231a
18. Vollmer AC, Belkin S, Smulski DR et al (1997) Detection of DNA damage by use of *Escherichia coli* carrying *recA'*::*lux*, *uvrA'*::*lux*, or *alkA'*::*lux* reporter plasmids. Appl Environ Microbiol 63:2566–2577. https://doi.org/10.1128/aem.63.7.2566-2571.1997
19. Gao G, Fan L, Lu H et al (2008) Engineering *Deinococcus radiodurans* into biosensor to monitor radioactivity and genotoxicity in environment. Sci Bull 53:1675–1681. https://doi.org/10.1007/s11434-008-0224-6
20. Gao Y, Wu K, Suo Z (2019) Photodetachable adhesion. Adv Mater 31:e1806948. https://doi.org/10.1002/adma.201806948
21. Porter GC, Schwass DR, Tompkins GR et al (2021) AgNP/Alginate nanocomposite hydrogel for antimicrobial and antibiofilm applications. Carbohydr Polym 251:117017. https://doi.org/10.1016/j.carbpol.2020.117017
22. Yuk H, Varela CE, Nabzdyk CS et al (2019) Dry double-sided tape for adhesion of wet tissues and devices. Nature 575:169–174. https://doi.org/10.1038/s41586-019-1710-5
23. Noor N, Shapira A, Edri R et al (2019) 3D printing of personalized thick and perfusable cardiac patches and hearts. Adv Sci 6:1900344. https://doi.org/10.1002/advs.201900344
24. Jang J, Lee J, Seol YJ et al (2013) Improving mechanical properties of alginate hydrogel by reinforcement with ethanol treated polycaprolactone nanofibers. Compos B Eng 45:1216–1221. https://doi.org/10.1016/j.compositesb.2012.09.059
25. Barakat A, Kamoun EA, El-Moslamy SH et al (2022) Photocurable carboxymethylcellulose composite hydrogel as a promising biomaterial for biomedical applications. Int J Biol Macromol 207:1011–1021. https://doi.org/10.1016/j.ijbiomac.2022.03.201
26. Ye W, Li H, Yu K et al (2020) 3D printing of gelatin methacrylate-based nerve guidance conduits with multiple channels. Mater Des 192:108757. https://doi.org/10.1016/j.matdes.2020.108757
27. Liu J, Qu M, Wang C et al (2022) A dual-cross-linked hydrogel patch for promoting diabetic wound healing. Small 18:e2106172. https://doi.org/10.1002/smll.202106172
28. Tsai CH, Hoang LN, Lin CC et al (2022) Evaluation of topical and subconjunctival injection of hyaluronic acid-coated nanoparticles for drug delivery to posterior eye. Pharmaceutics 14:1253–1269. https://doi.org/10.3390/pharmaceutics14061253
29. Yue K, Trujillo-de Santiago G, Alvarez MM et al (2015) Synthesis, properties, and biomedical applications of gelatin methacryloyl (GelMA) hydrogels. Biomaterials 73:254–271. https://doi.org/10.1016/j.biomaterials.2015.08.045
30. Chen S, Jang TS, Pan HM et al (2020) 3D freeform printing of nanocomposite hydrogels through in situ precipitation in reactive viscous fluid. Int J Bioprint 6:258–278. https://doi.org/10.18063/ijb.v6i2.258
31. Rastogi P, Kandasubramanian B (2019) Review of alginate-based hydrogel bioprinting for application in tissue engineering. Biofabrication 11:042001. https://doi.org/10.1088/1758-5090/ab331e
32. Stubbe B, Mignon A, Declercq H et al (2019) Development of gelatin-alginate hydrogels for burn wound treatment. Macromol Biosci 19:e1900123. https://doi.org/10.1002/mabi.201900123
33. Ye W, Xie C, Liu Y et al (2021) 3D printed high-resolution scaffold with hydrogel microfibers for providing excellent biocompatibility. J Biomater Appl 35:633–642. https://doi.org/10.1177/0885328220962606
34. Dubbin K, Dong Z, Park DM et al (2021) Projection microstereolithographic microbial bioprinting for engineered biofilms. Nano Lett 21:1352–1359. https://doi.org/10.1021/acs.nanolett.0c04100
35. Cai Y, Chang SY, Gan SW et al (2022) Nanocomposite bioinks for 3D bioprinting. Acta Biomater 151:45–69. https://doi.org/10.1016/j.actbio.2022.08.014
36. Kim SY, Han G, Hwang DB et al (2021) Design and usability evaluations of a 3D-printed implantable drug delivery device for acute liver failure in preclinical settings. Adv Healthc Mater 10:e2100497. https://doi.org/10.1002/adhm.202100497
37. Jang TS, Park SJ, Lee JE et al (2022) Topography-supported nanoarchitectonics of hybrid scaffold for systematically modulated bone regeneration and remodeling. Adv Funct Mater 32(51):2206863. https://doi.org/10.1002/adfm.202206863

38. Muskan, Gupta D, Negi NP (2022) 3D bioprinting: printing the future and recent advances. Bioprinting 27:e00211. https://doi.org/10.1016/j.bprint.2022.e00211
39. Yang X, Li S, Ren Y et al (2022) 3D printed hydrogel for articular cartilage regeneration. Compos B Eng 237:109863. https://doi.org/10.1016/j.compositesb.2022.109863
40. Han WT, Jang T, Chen S et al (2019) Improved cell viability for large-scale biofabrication with photo-crosslinkable hydrogel systems through a dual-photoinitiator approach. Biomater Sci 8:450–461. https://doi.org/10.1039/c9bm01347d
41. Kyle S (2018) 3D printing of bacteria: the next frontier in biofabrication. Trends Biotechnol 36:340–341. https://doi.org/10.1016/j.tibtech.2018.01.010
42. Freyman MC, Kou T, Wang S et al (2020) 3D printing of living bacteria electrode. Nano Res 13:1318–1323. https://doi.org/10.1007/s12274-019-2534-1
43. Shen J, Liu J, Yu S et al (2021) Diaminodiacid bridge improves enzymatic and in vivo inhibitory activity of peptide CPI-1 against botulinum toxin serotype A. Chin Chem Lett 32:4049–4052. https://doi.org/10.1016/j.cclet.2021.03.055
44. Ning W, Shang P, Wu J et al (2018) Novel amphiphilic, biodegradable, biocompatible, thermo-responsive ABA triblock copolymers based on PCL and PEG analogues via a combination of ROP and RAFT: synthesis, characterization, and sustained drug release from self-assembled micelles. Polymers 10:214–231. https://doi.org/10.3390/polym10020214
45. Blanchard L, de Groot A (2021) Coexistence of SOS-dependent and SOS-independent regulation of DNA repair genes in radiation-resistant *Deinococcus* bacteria. Cells 10:924–936. https://doi.org/10.3390/cells10040924
46. Prada Medina CA, Aristizabal Tessmer ET, Quintero Ruiz N et al (2016) Survival and SOS response induction in ultraviolet B irradiated *Escherichia coli* cells with defective repair mechanisms. Int J Radiat Biol 92:321–328. https://doi.org/10.3109/09553002.2016.1152412
47. Maslowska KH, Makiela-Dzbenska K, Fijalkowska IJ (2019) The SOS system: a complex and tightly regulated response to DNA damage. Environ Mol Mutagen 60:368–384. https://doi.org/10.1002/em.22267
48. Lippincott-Schwartz J, Snapp E, Kenworthy A (2001) Studying protein dynamics in living cells. Nat Rev Mol Cell Biol 2:444–456. https://doi.org/10.1038/35073068
49. Schaffner M, Rühs P, Coulter F et al (2017) 3D printing of bacteria into functional complex materials. Sci Adv 3:6804. https://doi.org/10.1126/sciadv.aao6804
50. Song K, Compaan AM, Chai W et al (2020) Injectable gelatin microgel-based composite ink for 3D bioprinting in air. ACS Appl Mater Interfaces 12:22453–22466. https://doi.org/10.1021/acsami.0c01497
51. Asohan AW, Hashim R, Ku Ishak KM et al (2022) Preparation and characterisation of cellulose nanocrystal/alginate/polyethylene glycol diacrylate (CNC/Alg/PEGDA) hydrogel using double network crosslinking technique for bioprinting application. Appl Sci 12:771–786. https://doi.org/10.3390/app12020771
52. He Y, Yang F, Zhao H et al (2016) Research on the printability of hydrogels in 3D bioprinting. Sci Rep 6:29977. https://doi.org/10.1038/srep29977